BMC Cardiovascular Disorders

RESEARCH

Open Access

# Quantitative evaluation of radiation-induced heart disease in beagle dogs by speckle tracking echocardiography

Zi-Ying Wang[1†], Long Huang[2†], Li-Qun Li[3], Chun-Quan Zhang[1], Liang-Yun Guo[1], Yan-Na Liu[1] and Ling-Min Liao[1*]

## Abstract

**Objective** This study aimed to detect early changes in left ventricular systolic function in Beagle dogs after radiotherapy using two-dimensional speckle tracking echocardiography and to explore its potential value in evaluating radiation-induced heart disease.

**Methods** Thirty-six Beagle dogs were randomized into a control group ($n=18$) and an irradiation group ($n=18$). The irradiation group received a single dose of 20 Gy to the left ventricular anterior wall, while controls underwent sham irradiation. Conventional echocardiography and 2D speckle tracking echocardiography were performed at baseline and 3, 6, and 12 months post-procedure. Additionally, six dogs were randomly selected from each group and euthanized at 3-, 6-, and 12-month post-irradiation, and their hearts were collected for histopathological testing.

**Results** In the irradiation group, the global longitudinal strain of the left ventricle and regional strain in the irradiated area were significantly reduced versus baseline and controls by 3 months, with progressive decline at 6 and 12 months. Strain reduction correlated spatially with pathological injury. Conversely, there were no substantial differences in conventional echocardiographic parameters between the groups after 3 months. Conventional parameters (e.g., LVEF) showed differences only at later timepoints. Histopathology revealed progressive cardiomyocyte damage, fibrosis, and microvascular injury in irradiated regions, extending to the posterior wall by 12 months.

**Conclusion** Two-dimensional speckle tracking echocardiography-derived strain parameters spatially correlate with radiation-induced pathological changes and detect subtle systolic dysfunction prior to irreversible remodeling. Speckle tracking may localize regions of peak radiation dose delivery.

**Keywords** Radiotherapy, Radiation-induced heart disease, Speckle tracking echocardiography, Ultrasound

†Zi-Ying Wang and Long Huang contributed equally to this work as co-first authors.

*Correspondence:
Ling-Min Liao
liaolingmin85@163.com
[1] Department of Ultrasound, The Second Affiliated Hospital, Jiangxi Medical College, Nanchang University, Nanchang, China
[2] Department of Oncology, The Second Affifiliated Hospital, Jiangxi Medical College, Nanchang University, Nanchang, China
[3] Department of Ultrasound, Yanshan County People's Hospital, Yanshan, Jingxi, China

## Introduction

Radiotherapy is an essential component of cancer treatment [1]. Nevertheless, surrounding normal tissues inevitably receive incidental radiation exposure during therapeutic delivery [2–5]. Of particular concern are thoracic malignancies, where cardiac irradiation may induce structural damage to the pericardium, myocardium, valves, coronary vasculature, and conduction system– a constellation of injuries collectively termed radiation-induced heart disease (RIHD). First documented in the 1920s [6], RIHD initially garnered limited clinical attention due to the short life expectancy of cancer patients in that era. However, advances in oncologic therapies have markedly improved long-term survival rates, allowing RIHD to emerge as a leading contributor to late mortality in this population [2, 7–10]. While radiotherapy confers demonstrable survival benefits, its therapeutic value may be counterbalanced by an increased risk of RIHD [11–14], which has been reported in 10–30% of patients who undergo radiotherapy [15–17]. Despite consensus recommendations from oncology and cardiology societies for routine RIHD surveillance in thoracic radiotherapy recipients, standardized protocols for early detection and longitudinal monitoring remain undefined [18–20]. Emerging evidence suggests that 2D-STE enables detection of subclinical myocardial injury prior to overt functional decline. Notably, global longitudinal strain (GLS) – a STE-derived parameter – demonstrates superior sensitivity and specificity over conventional echocardiographic indices like left ventricular ejection fraction (LVEF) in identifying early RIHD [21]. This study employed a Beagle dog model of RIHD to 1) characterize temporal patterns of left ventricular strain alterations and histopathological progression, and 2) evaluate the clinical utility of two-dimensional speckle tracking echocardiography (2D-STE) for early disease identification, monitoring, and cardiotoxicity risk stratification.

## Materials and methods

The number of animals utilized in this study adhered to the Guidelines for Animal Experiments of Nanchang University and received approval from the Ethics Committee of the same institution. Furthermore, the research was conducted and reported in compliance with the Animal Research: Reporting of In Vivo Experiments (ARRIVE) guidelines.

### Animals

A total of thirty-six male Beagle dogs, each twelve months old and weighing an average of 12.77 ± 0.83 kg, were procured from the Institute of Experimental Animals and were individually housed in stainless steel cages within an air-conditioned environment at the Experimental Animal Center of Nanchang University. These Beagles were fed a standard dog chow twice daily. Thirty-six Beagle dogs were randomly assigned to a control group ($n=18$) and an irradiation group ($n=18$). Following the administration of anesthesia using sodium pentobarbital at a dosage of 30 mg/kg, the irradiation group received a localized dose of 20 Gy to the anterior wall of the left ventricle. In contrast, the control group underwent sham irradiation. When short-term signs of pain were observed, appropriate intervention strategies, including analgesics or additional anesthesia, were implemented. Daily observations were made to record the diet of all the beagles (weight of dog chow remaining each day) and their mental status. Indicators of abnormal mental status included reduced appetite, reluctance to move, restlessness, unresponsiveness to external stimuli, anxiety, barking, walking aimlessly, and turning around. All dogs underwent conventional echocardiography and 2D-STE 1 week before irradiation and 3, 6, and 12 months after sham or local irradiation. Body weight and heart rate were also recorded at these intervals. Additionally, six dogs were randomly selected from each group and euthanized using carbon dioxide at 3, 6, and 12 months after irradiation, with their hearts subsequently collected for pathological testing.

### Heart irradiation

All beagle dogs were subjected to anesthesia via intravenous administration of 3% pentobarbital sodium at a dosage of 30 mg/kg. They have no corneal reflex but can breathe on their own. All animals were positioned in a supine orientation on a CT-simulated locator (GE Discovery CT590) for a control-enhanced CT simulation scan. All positioning images were subsequently transmitted to an Elekta MC TPS system (Varian). The anterior wall of the left ventricle was meticulously delineated layer by layer as the irradiation target (referring to the 17-segment division method of the left ventricle and expanding 3 mm). A conformal intensity-modulated radiation therapy plan was developed by a physicist and executed using a linear accelerator. The beagle dogs in the irradiation group received a single dose of of irradiation with 6-MV X-rays, while those in the control group underwent the identical procedure but without the application of irradiation.

### Biochemical index determination

Serum cTnI was detected as a cardiac function index by small saphenous vein blood of the hind legs of all beagles before each ultrasound examination.

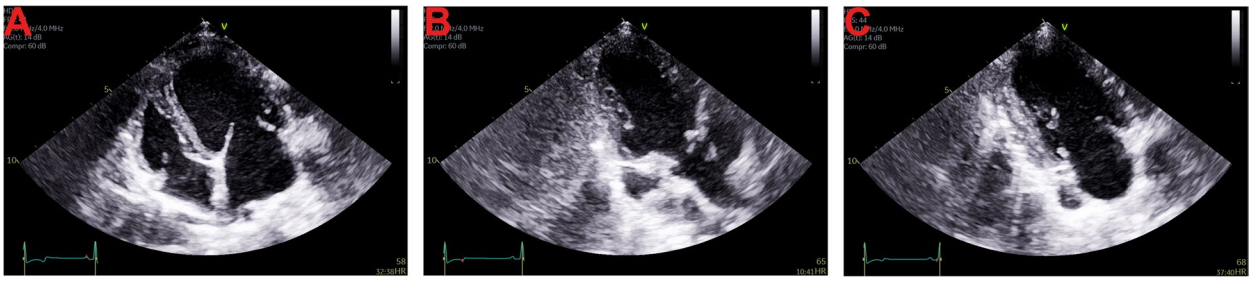

**Fig. 1** Four-chamber (**A**), three-chamber (**B**) and two-chamber (**C**) standard cross-sections of beagle dogs

### Conventional echocardiographic assessment

All dogs were anesthetized via intravenous administration of 3% pentobarbital sodium at a dosage of 30 mg/kg. Subsequently, they were positioned in the left lateral recumbent position and secured to an examination table equipped with an electrocardiogram monitor. Conventional parameters were assessed utilizing the S5-1 heart probe of a color Doppler ultrasound scanner (GE Vivid E95). All the recorded images were measured using the same diagnostic ultrasound apparatus, and the mean values derived from three consecutive heartbeats were used as the measurement values. In the B-mode LV short-axis view at the level of the papillary muscle, parameters including the interventricular septum end-diastolic dimension (IVSD), left ventricular posterior wall end-diastolic dimension (LVPWD), left ventricular end-diastolic diameter (LVEDD) and left ventricular end-systolic diameter (LVESD) were measured using the leading edge-to-leading edge method [22]. Then, the left ventricular end-diastolic volume (LVEDV), left ventricular end-systolic volume (LVESV), and LVEF were calculated. In the left apical 4-chamber view, the early diastolic peak velocity (peak E), the late diastolic peak flow velocity (peak A) of the mitral orifice and the ratio of peak E to peak A (E/A) were calculated.

### 2D-STE assessment

Continuous acquisition of two-dimensional dynamic images of the standard apical four-chamber view, the standard apical two-chamber view and the standard apical long-axis view of the left ventricle at a frame rate of 57 frames per second, with data collection spanning for 3–5 cardiac cycles (Fig. 1). The image data were subsequently transmitted to the EchoPAC workstation, where the GLS and LS of the left ventricular myocardium were evaluated using 2D-STE analysis software. The incidence of subclinical cardiac dysfunction in beagles (defined as a relative decrease in GLS > 15% during cancer treatment) was recorded at different time points.

### Histopathological assessment

The dogs were subjected to anesthesia and subsequently euthanized using carbon dioxide. Following this procedure, the chest cavity was dissected, and the heart was swiftly excised for examination of surface and morphological abnormalities. The left ventricular tissue was then immersed and immobilized in 10% formalin for histopathological analysis. For each heart, myocardial samples was collected from the anterior wall (irradiated area) and the posterior wall (less irradiated area) at the middle level of the left ventricle. All tissue specimens underwent fixation, trimming, washing, and progressive dehydration in ethanol, followed by paraffin embedding for serial sectioning. Four-micron-thick sections were prepared and stained using hematoxylin–eosin (HE, Servicebio), wheat germ agglutinin (WGA, SIGMA), Masson trichrome (Servicebio), and CD34 immunostaining (Servicebio) [23–26].

Five nonvascular microscopic fields (×400) were randomly selected from the HE-stained slices to evaluate myocardial degeneration. The degree of myocardial degeneration was graded as 0 (normal: no degeneration of myocardial cells), 1 (mild: < 20% degeneration of myocardial cells, mainly manifesting as individual cardiomyocyte edema and no necrosis), 2 (moderate: 20%–50% degeneration of myocardial cells, mainly manifesting as clusters of cardiomyocyte edema and focal necrosis), and 3 (severe: > 50% degeneration of myocardial cells, mainly manifesting as diffuse cardiomyocyte edema and patchy necrosis) [23].

Five vascular microscopic fields (400×) were randomly selected from the HE stained slices to evaluate myocardial vascular injury. The degree of myocardial vascular injury was graded as 0(no fibrosis: adventitia thickness≈half the media), 1(mild fibrosis: adventitia thickness≈the media), 2(moderate fibrosis: adventitia thickness≈ 2×the media), 3(severe fibrosis: adventitia thickness ≥ 3×the media) [24].

Five independent microscopic fields (400×) were randomly selected from the WGA-stained slices to evaluate

**Table 1** Comparison of serum cTnI concentration between the control and irradiation groups ($\bar{x} \pm s$)

| Grouping | 1 week before irradiation | 3 month after irradiation | 6 month after irradiation | 12 month after irradiation | P |
|---|---|---|---|---|---|
| Control group (ng/ml) | 0. 27 ± 0. 05 | 0. 26 ± 0. 04 | 0. 27 ± 0. 03 | 0. 28 ± 0. 09 | 0. 714 |
| Irradiation group (ng/ml) | 0. 27 ± 0. 04 | 0. 29 ± 0. 08 | 0. 28 ± 0. 04 | 0. 26 ± 0. 05 | 0. 563 |
| P | 0. 809 | 0. 06 | 0. 447 | 0. 614 | |

myocardial cell size [25]. The green fluorescence indicates the cell membrane, and the surface area of cardiomyocytes was measured by ImageJ software.

Five independent microscopic fields (400×) were randomly selected from the Masson-stained sections to evaluate cardiac interstitial fibrosis. The extent and degree of fibrosis were subjectively graded on a scale of 0 to 4. Grade 0 indicated no obvious proliferation of collagen fibers except for small islands of fibrous tissue around the capillaries and an intercellular single layer of collagenous tissue, as in normal myocardium. Focal and minimal fibrosis were graded as 1, mild patchy fibrosis as 2, moderate diffuse fibrosis as 3, and the most prominent fibrosis covering a large area of the specimen as 4 [26].

#### 2D-STE repeatability test

The 2D-STE data of 10 beagle dogs randomly selected from the two groups were analyzed twice at 1-week intervals by one investigator for intraobserver reproducibility. Interobserver repeatability assessment was performed by analyzing 2D-STE data from 10 beagle dogs randomly selected from two groups by two independent investigators. The investigators were blinded to the other measurements.

#### Statistical analysis

SPSS26. 0 software package (SPSS, Inc., Chicago, IL, USA) was used for the statistical analysis. The descriptive statistical results of the continuous variables are expressed as the mean ± standard deviation. Differences in continuous variables between groups were tested using t tests and ANOVA. Differences in discontinuous variables between groups were tested using the rank-sum test. Bland-Atlman analysis was used to evaluate the intraobserver and interobserver consistency. Inter- and intraobserver repeatability values were evaluated using the intraclass correlation coefficient (ICC). Statistical tests were two-sided, and $P < 0.05$ was considered to indicate statistical significance.

## Results

### Animal growth

All beagle dogs completed the experiment successfully. The mean weights of the dogs in the control group at 1 week before irradiation and 3, 6, and 12 months after irradiation were recorded as 12. 8 ± 0. 8 kg, 13. 6 ± 0. 8 kg, 14. 2 ± 0. 6 kg, and 15. 0 ± 0. 6 kg, respectively. In comparison, the irradiation group exhibited average weights of 12.9 ± 0.6 kg, 13.6 ± 0.7 kg, 14.0 ± 0.7 kg, and 13.8 ± 0.7 kg at the same time intervals respectively. No significant differences were observed in weight, diet intake, heart rate, activity levels, or mental status between the two groups before irradiation or at 3 or 6 months after irradiation. However, at 12 months after irradiation, the beagle dogs in the irradiation group demonstrated a statistically significant weight reduction ($P = 0.036$) than those in the control group. And after 3 months of irradiation, half of the beagles in the irradiation group began to show a gradual decline in their food intake. All beagles exhibited a significant decrease in feeding, reluctance to move, and unresponsive to external stimuli by 12 months after irradiation.

### cTnI detection results

There were no significant differences in the serum cTnI concentration in the beagles between the control and irradiation groups before irradiation or at 3, 6, or 12 months after irradiation (Table 1).

### Left ventricular function

There were no significant differences in heart rate, IVS, LVPWD, LVEDD, LVESD, LVEDV, LVESV or LVEF between the control and irradiation groups 1 week before irradiation or 3 months after irradiation. The LVESV was greater ($P = 0.006$), and the LVEF was lower ($P = 0.007$) than in the control group at 6 months after irradiation. Both LVEDV ($P = 0.007$) and LVESV ($P < 0.001$) were significantly greater in the irradiation group than in the control group, and the LVEF ($P < 0.001$) was significantly lower at 12 months after irradiation (Table 2).

No obvious abnormal motion of the left ventricular wall was detected in either the control or irradiation groups 1 week before irradiation or 3 or 6 months after irradiation. However, at 12 months after irradiation, abnormal motion of the regional left ventricular wall was noted in or adjacent to the irradiation site within the irradiation group.

**Table 2** Comparison of functional parameters of left ventricle between the control and irradiation groups ($\bar{x} \pm s$)

| Parameter | 1 week before irradiation | 3 month after irradiation | 6 month after irradiation | 12 month after irradiation | P |
|---|---|---|---|---|---|
| Heart rate (bpm) | | | | | |
| Control group | 54.33 ± 6.38 | 54.89 ± 4.95 | 56.75 ± 6.55 | 53.00 ± 3.69 | 0.56 |
| Irradiation group | 55.06 ± 5.46 | 53.94 ± 4.93 | 54.33 ± 4.91 | 54.33 ± 5.32 | 0.93 |
| P | 0.72 | 0.57 | 0.32 | 0.63 | |
| IVSD (mm) | | | | | |
| Control group | 4. 21 ± 0. 46 | 4. 24 ± 0. 39 | 4. 25 ± 0. 45 | 4. 23 ± 0. 37 | > 0. 99 |
| Irradiation group | 4. 12 ± 0. 41 | 4. 13 ± 0. 44 | 4. 22 ± 0. 42 | 4. 25 ± 0. 47 | 0. 86 |
| P | 0. 50 | 0. 43 | 0. 85 | 0. 95 | |
| LVPWD (mm) | | | | | |
| Control group | 4. 77 ± 0. 44 | 4. 81 ± 0. 47 | 4. 83 ± 0. 43 | 4. 73 ± 0. 44 | 0. 97 |
| Irradiation group | 4. 73 ± 0. 45 | 4. 76 ± 0. 38 | 4. 72 ± 0. 45 | 4. 80 ± 0. 49 | 0. 98 |
| P | 0. 79 | 0. 76 | 0. 52 | 0. 81 | |
| LVEDD (mm) | | | | | |
| Control group | 32. 88 ± 2. 95 | 32. 78 ± 2. 18 | 32. 92 ± 1. 88 | 32. 33 ± 1.37 | 0. 96 |
| Irradiation group | 33. 28 ± 2. 80 | 32. 83 ± 2. 33 | 33. 08 ± 2. 75 | 33. 83 ± 2. 32 | 0. 86 |
| P | 0. 69 | 0. 94 | 0. 86 | 0. 20 | |
| LVESD (mm) | | | | | |
| Control group | 20. 55 ± 1. 79 | 20. 28 ± 1.27 | 21. 25 ± 1. 36 | 21.00 ± 1.41 | 0. 34 |
| Irradiation group | 21. 11 ± 1.45 | 20. 83 ± 0. 86 | 21.00 ± 0.95 | 20. 83 ± 1. 47 | 0. 90 |
| P | 0. 31 | 0. 13 | 0. 61 | 0. 85 | |
| LVEDV (ml) | | | | | |
| Control group | 30. 06 ± 3. 73 | 29. 72 ± 2. 95 | 30. 08 ± 3. 78 | 30.00 ± 1. 41 | 0. 99 |
| Irradiation group | 31. 89 ± 3.85 | 30. 05 ± 2. 92 | 30. 58 ± 1. 93 | 34. 67 ± 3.08 | 0.04 |
| P | 0. 51 | 0. 74 | 0. 69 | 0.007 | |
| LVESV (ml) | | | | | |
| Control group | 10. 33 ± 1. 24 | 10. 55 ± 1.04 | 9. 92 ± 0. 79 | 10. 17 ± 0.75 | 0. 43 |
| Irradiation group | 10. 39 ± 1. 09 | 10. 39 ± 0. 91 | 11. 33 ± 1.37[#] | 14. 33 ± 1. 21* | < 0. 001 |
| P | 0. 90 | 0. 61 | 0.006 | P < 0. 001 | |
| LVEF (%) | | | | | |
| Control group | 65. 43 ± 3. 49 | 64. 40 ± 2. 67 | 66. 75 ± 3. 30 | 66. 08 ± 2. 43 | 0. 23 |
| Irradiation group | 66. 06 ± 3. 57 | 65. 14 ± 2. 67 | 62. 46 ± 3.70[#] | 58. 61 ± 1. 67[*] | < 0. 001 |
| P | 0. 60 | 0. 41 | 0.007 | < 0. 001 | |
| E/A | | | | | |
| Control group | 1. 46 ± 0. 06 | 1. 48 ± 0. 06 | 1. 52 ± 0. 05 | 1. 51 ± 0. 05 | 0. 12 |
| Irradiation group | 1. 43 ± 0. 06 | 1. 39 ± 0. 09[#] | 1. 23 ± 0. 07[*] | 0. 98 ± 0. 10[*] | < 0. 001 |
| P | 0. 12 | 0.001 | < 0. 001 | < 0. 001 | |

[#] represent comparison with before irradiation, $P < 0.05$; [*]represent $P < 0.001$

Additionally, a minor pericardial effusion was observed in two beagles from the irradiation group at 3 months after irradiation; this effusion subsequently resolved. And the local pericardial echo of the anterior left ventricular wall was enhanced at 6 months after irradiation.

#### Longitudinal strain of the left ventricle in 2D-STE

The EchoPAC software systematically segmented the left ventricular myocardium into 17 segments, tracked each segment and finally displayed the strain curve and bull's eye diagram. In the control group of beagles, there was no significant reduction in the area of LS at 3, 6 or 12 months after irradiation (Fig. 2). Conversely, in the irradiation group, a progressive decline in the LS was noted within both the irradiated area and adjacent areas, and the extent of this decline gradually increased over time (Fig. 3).

Univariate ANOVA indicatedc that there was no significantly change in the GLS of the left ventricle and the

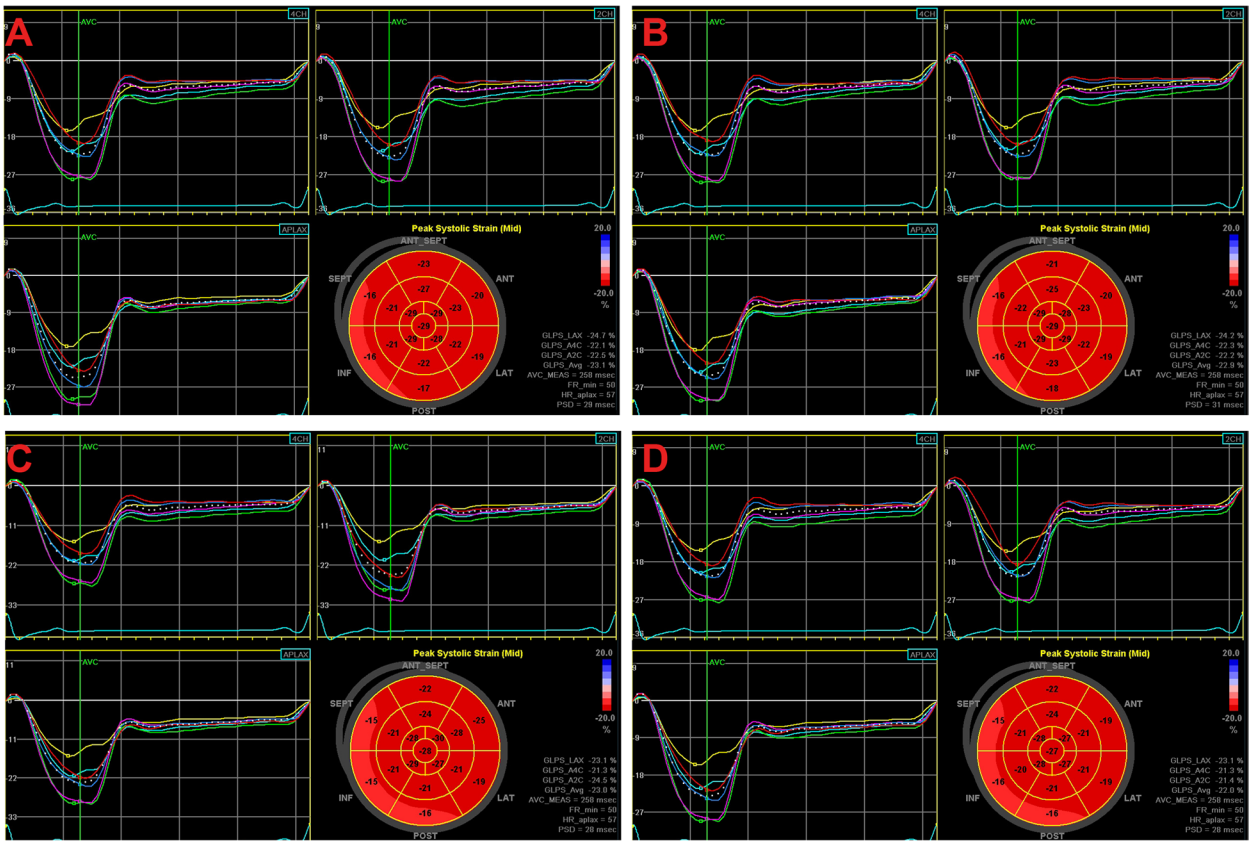


**Fig. 2** Longitudinal strain diagram of 17 segments of left ventricle at each time point before and after irradiation in the control group with 2D-STE (**A** 1 week before irradiation, **B** 3 month after irradiation, **C** 6 month after irradiation, **D** 12 month after irradiation)

LS of each segment in the control group at any time point before or after irradiation ($P > 0.05$). In contrast, the GLS and LS of the irradiated area gradually decreased in the irradiation group after irradiation ($P < 0.001$).

When compared to the control group and baseline measurements, the GLS and LS in the irradiated area were significantlydiminished in the irradiation group at 3 months after irradiation ($P < 0.001$), with further decreased observed at 6 months after irradiation ($P < 0.001$), and increased extent decline noted at 12 months after irradiation ($P < 0.001$) (Table 3).

Notably, none of the beagles in the irradiation group exhibited signs of subclinical cardiac dysfunction after 3 months of irradiation. After 6 months of irradiation, four beagles in the irradiation group demonstrated a relative decrease in GLS of > 15%. By 12 months of irradiation, all six remaining beagles in the irradiation group presented with subclinical cardiac dysfunction (Table 4).

### Histologic results

Examinations of the heart surface in euthanized beagles indicated no discernible abnormalities in the hearts of the control group at 3, 6 or 12 months after irradiation. Conversely, in the irradiation group, the cardiac surface in the irradiated region exhibited a whitish appearance at 3 months after irradiation and became hardened at 6 and 12 months after irradiation, which was markedly distinct from the nonirradiated area.

HE staining did not reveal any significant abnormalities in the myocardial tissue of the control group at 3, 6, or 12 months after irradiation (Fig. 4A, B, C). In contrast, the irradiated area of the irradiation group displayed notable pathological alterations when compared to the control group. At 3 months after irradiation, the irradiated area showed mild myocardial degeneration, mild myocardial interstitial fibrosis, mild hyperplasia of fibrous tissue, and thickening of the walls of small interstitial vessel (Fig. 4D). By 6 months after irradiation, the irradiated area demonstrated moderate myocardial degeneration with disorganized arrangement, moderate myocardial interstitial fibrosis, and obvious thickening of the interstitial small vessel wall (Fig. 4E). At 12 months after irradiation, the irradiated area presented with patchy necrosis of cardiomyocytes, severe myocardial interstitial fibrosis, and significant thickening or luminal stenosis of interstitial small vessel walls (Fig. 4F). There

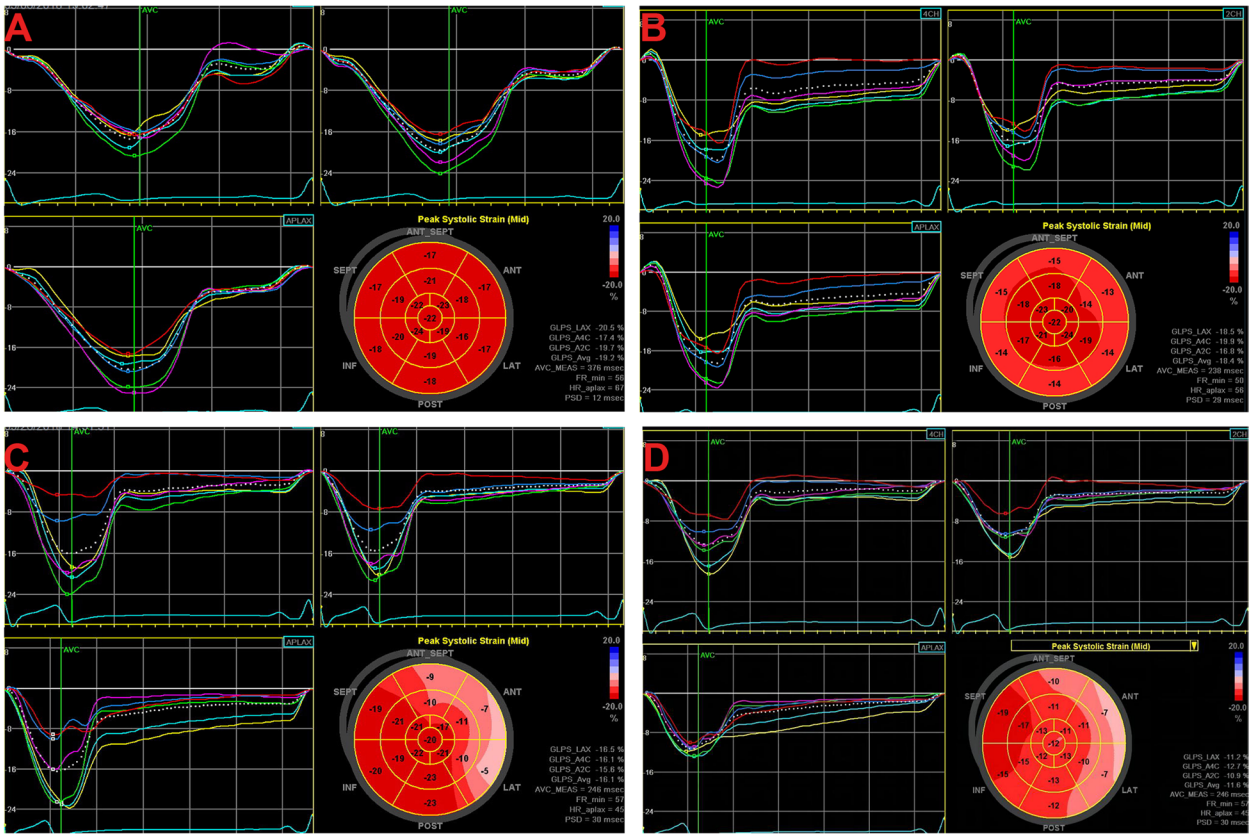


**Fig. 3** Longitudinal strain diagram of 17 segments of left ventricle at each time point before and after irradiation in the irradiation group with 2D-STE(**A** 1 week before irradiation, **B** 3 month after irradiation, **C** 6 month after irradiation, **D** 12 month after irradiation)

were statistically significant differences in the myocardial degeneration score and vascular injury score between the two groups at 3, 6, and 12 months after irradiation (Table 5).

WGA showed that cardiomyocytes in the control group exhibited uniform size and orderly arrangement at 3, 6, and 12 months after irradiation (Fig. 5A, B, C). Compared with the control group, the cardiomyocytes in the irradiated group displayed a slight increase in size and a more disordered at 3 months after irradiation (Fig. 5D). By 6 months after irradiation, the cardiomyocytes in the irradiated area were significantly larger and exhibited a greater degree of disorganization (Fig. 5E). At 12 months after irradiation, the cardiomyocytes were severely deformed and uneven in size, and the myocardial texture was largely absent (Fig. 5F).

Masson staining indicated that the control group exhibited no obvious abnormalities ( grade 0) after irradiation (Fig. 6A, B, C). However, there was a progressive exacerbation of myocardial interstitial fibrosis in the irradiated area of the irradiation group,with grade of 1, 2, and 3 observed at 3, 6, and 12 month after irradiation,, respectively (Fig. 6D, E, F).

### The relationship between 2D-STE parameters and histological results

The strain results showed high concordance with the pathologic findings. The left ventricular anterior wall segments within the irradiated region were the first to exhibit changes. Notably, the GLS of the basal, mid, apical of the anterior wall showed a significant reduction after 3 months of irradiation, coinciding with observable alterations in the myocardial histopathology of the anterior wall. And no significant changes were noted in the posterior wall during this period. After 12 months of irradiation, the extent of strain-segment injury in the irradiated cohort of beagles increased, affecting both the posterior and lateral walls. At this juncture, significant alterations in myocardial injury were evident in the myocardial tissue of both the anterior and posterior walls.

### Interobserver and intraobserver repeatability

The interobserver agreement assessed by the ICC was 0. 82, 0. 91 and 0. 85 for GLS, LVEDV and LVESV, respectively (Table 6), whereas the intraobserver agreement

**Table 3** Comparison of GLS of Left Ventricle and LS of Each Segment Between the Control and Irradiation Groups ($\bar{x} \pm s$)

| Parameter | 1 week before irradiation | 3 month after irradiation | 6 month after irradiation | 12 month after irradiation | P |
|---|---|---|---|---|---|
| Base segment of anterior wall (%) | | | | | |
| Control group | 18. 61 ± 1. 53 | 18. 89 ± 2. 29 | 18. 42 ± 1. 55 | 18. 67 ± 3. 70 | 0. 869 |
| Irradiation group | 17. 83 ± 1. 34 | 13. 83 ± 3. 06* | 12. 5 ± 2. 06* | 9. 83 ± 1. 34* | *P* < 0. 001 |
| P | 0. 125 | *P* < 0. 001 | *P* < 0. 001 | *P* < 0. 001 | |
| Mid segment of anterior wall (%) | | | | | |
| Control group | 18. 89 ± 1. 33 | 18. 67 ± 1. 60 | 18. 67 ± 2. 91 | 19 ± 1. 91 | 0. 924 |
| Irradiation group | 18. 61 ± 0. 95 | 14. 44 ± 3. 42* | 12. 58 ± 1. 93* | 9. 5 ± 2. 71* | *P* < 0. 001 |
| P | 0. 488 | *P* < 0. 001 | *P* < 0. 001 | *P* < 0. 001 | |
| Apex segment of anterior wall (%) | | | | | |
| Control group | 20. 28 ± 0. 98 | 20. 5 ± 3. 17 | 20. 33 ± 1. 11 | 20. 17 ± 2. 07 | 0. 907 |
| Irradiation group | 20. 17 ± 0. 96 | 17. 56 ± 1. 61* | 14. 92 ± 2. 18* | 10 ± 0. 82* | *P* < 0. 001 |
| P | 0. 741 | *P* < 0. 001 | *P* < 0. 001 | *P* < 0. 001 | |
| Base segment of anterior septum (%) | | | | | |
| Control group | 18. 67 ± 1. 20 | 18. 72 ± 0. 93 | 19. 08 ± 2. 11 | 19. 17 ± 0. 69 | 0. 618 |
| Irradiation group | 18. 17 ± 3. 38 | 15. 67 ± 2. 11* | 14. 25 ± 1. 42* | 13. 17 ± 1. 34# | P < 0. 001 |
| P | 0. 269 | *P* < 0. 001 | *P* < 0. 001 | *P* < 0. 001 | |
| Mid segment of anterior septum (%) | | | | | |
| Control group | 20. 06 ± 1. 18 | 19. 39 ± 4. 21 | 19. 67 ± 1. 10 | 19. 5 ± 0. 96 | 0. 403 |
| Irradiation group | 20. 33 ± 2. 15 | 18. 28 ± 1. 24* | 17. 08 ± 3. 55* | 15. 5 ± 1. 26* | *P* < 0. 001 |
| P | 0. 492 | *P* < 0. 05 | *P* < 0. 001 | *P* < 0. 001 | |
| Base segment of lateral wall (%) | | | | | |
| Control group | 17. 5 ± 3. 42 | 17. 56 ± 1. 67 | 17. 67 ± 2. 11 | 18 ± 1. 29 | 0. 908 |
| Irradiation group | 17. 56 ± 1. 34 | 14. 56 ± 1. 4* | 13. 75 ± 1. 42* | 12. 83 ± 4. 52# | *P* < 0. 001 |
| P | 0. 907 | *P* < 0. 001 | *P* < 0. 001 | *P* < 0. 001 | |
| Mid segment of lateral wall (%) | | | | | |
| Control group | 18 ± 1. 15 | 18. 22 ± 1. 84 | 18. 5 ± 1. 26 | 18. 83 ± 2. 46 | 0. 648 |
| Irradiation group | 17. 94 ± 1. 22 | 15. 94 ± 3. 08* | 13. 92 ± 1. 18* | 11. 83 ± 1. 07* | *P* < 0. 001 |
| P | 0. 892 | *P* < 0. 001 | *P* < 0. 001 | *P* < 0. 001 | |
| Apex segment of lateral wall (%) | | | | | |
| Control group | 20. 5 ± 1. 64 | 19. 78 ± 1. 58 | 19. 83 ± 1. 06 | 20. 33 ± 1. 70 | 0. 504 |
| Irradiation group | 20. 17 ± 1. 54 | 19. 17 ± 1. 25 | 17. 08 ± 2. 44* | 15 ± 3. 29* | *P* < 0. 001 |
| P | 0. 545 | 0. 261 | *P* < 0. 001 | *P* < 0. 001 | |
| Base segment of posterior wall (%) | | | | | |
| Control group | 18. 39 ± 3. 11 | 19 ± 0. 94 | 18. 58 ± 2. 44 | 18. 5 ± 1. 26 | 0. 484 |
| Irradiation group | 18. 72 ± 1. 24 | 18. 67 ± 3. 1 | 17. 08 ± 1. 80# | 15. 83 ± 4. 34* | *P* < 0. 001 |
| P | 0. 541 | 0. 422 | 0. 068 | *P* < 0. 05 | |
| Mid segment of posterior wall (%) | | | | | |
| Control group | 20. 33 ± 0. 88 | 20. 05 ± 1. 22 | 19. 92 ± 1. 55 | 19. 5 ± 2. 71 | 0. 579 |
| Irradiation group | 20. 06 ± 0. 91 | 20. 17 ± 1. 07 | 18 ± 2. 19# | 16. 16 ± 1. 06* | *P* < 0. 001 |
| P | 0. 453 | 0. 440 | *P* < 0. 05 | *P* < 0. 001 | |
| Base segment of inferior wall (%) | | | | | |
| Control group | 19. 17 ± 1. 5 | 19. 56 ± 1. 42 | 18. 92 ± 0. 95 | 19. 17 ± 1. 34 | 0. 660 |
| Irradiation group | 19 ± 1. 33 | 19. 11 ± 1. 20 | 19. 08 ± 0. 76 | 16. 83 ± 1. 34# | *P* < 0. 05 |
| P | 0. 638 | 0. 184 | 0. 826 | *P* < 0. 05 | |
| Mid segment of inferior wall (%) | | | | | |
| Control group | 20. 05 ± 1. 35 | 20. 22 ± 0. 97 | 20. 25 ± 1. 09 | 20. 17 ± 1. 67 | 0. 974 |
| Irradiation group | 19. 83 ± 2. 34 | 20 ± 1. 75 | 19. 67 ± 0. 94 | 16. 8 ± 1. 34* | *P* < 0. 001 |
| P | 0. 726 | 0. 564 | 0. 327 | *P* < 0. 05 | |

**Table 3** (continued)

| Parameter | 1 week before irradiation | 3 month after irradiation | 6 month after irradiation | 12 month after irradiation | P |
|---|---|---|---|---|---|
| Apex segment of inferior wall (%) | | | | | |
| Control group | 20. 55 ± 1. 53 | 20. 28 ± 2. 09 | 20 ± 1. 53 | 20. 83 ± 1. 67 | 0. 639 |
| Irradiation group | 20. 83 ± 1. 38 | 20. 56 ± 0. 89 | 19. 92 ± 1. 32 | 16. 5 ± 0. 96* | *P* < 0. 001 |
| P | 0. 481 | 0. 464 | 0. 99 | *P* < 0. 05 | |
| Base segment of posterior septum (%) | | | | | |
| Control group | 18. 28 ± 1. 32 | 18. 11 ± 1. 37 | 18. 42 ± 1. 38 | 18. 67 ± 0. 94 | 0. 834 |
| Irradiation group | 17. 94 ± 2. 47 | 17. 78 ± 0. 97 | 17. 5 ± 0. 96 | 16. 33 ± 1. 49# | 0. 064 |
| P | 0. 409 | 0. 586 | 0. 116 | *P* < 0. 05 | |
| Mid segment of posterior septum (%) | | | | | |
| Control group | 19. 78 ± 1. 08 | 19. 39 ± 1. 01 | 19. 08 ± 1. 19 | 19. 17 ± 2. 07 | 0. 369 |
| Irradiation group | 19. 33 ± 1. 15 | 19. 24 ± 0. 94 | 18. 41 ± 1. 04# | 17. 5 ± 0. 96# | 0. 001 |
| P | 0. 344 | 0. 820 | 0. 246 | *P* < 0. 05 | |
| Apex segment of septum (%) | | | | | |
| Control group | 21. 5 ± 1. 01 | 21. 11 ± 0. 87 | 20. 83 ± 1. 79 | 20. 67 ± 1. 25 | 0. 195 |
| Irradiation group | 21. 83 ± 0. 76 | 20. 78 ± 2. 31 | 19. 83 ± 0. 81* | 18 ± 0. 82* | *P* < 0. 001 |
| P | 0. 286 | 0. 390 | *P* < 0. 001 | *P* < 0. 001 | |
| Peak of apex (%) | | | | | |
| Control group | 20. 91 ± 3. 08 | 21 ± 1. 15 | 20. 42 ± 1. 11 | 21. 33 ± 1. 25 | 0. 402 |
| Irradiation group | 21. 11 ± 0. 74 | 20. 78 ± 1. 18 | 19. 25 ± 2. 09* | 16 ± 0. 82* | *P* < 0. 001 |
| P | 0. 347 | 0. 495 | *P* < 0. 05 | *P* < 0. 001 | |
| GLS (%) | | | | | |
| Control group | 20. 02 ± 0. 90 | 19. 61 ± 1. 10 | 19. 56 ± 0. 95 | 19. 6 ± 1. 54 | 0. 532 |
| Irradiation group | 19. 92 ± 0. 65 | 18. 49 ± 0. 82* | 17. 22 ± 0. 90* | 14. 17 ± 1. 66* | *P* < 0. 001 |
| P | 0. 555 | *P* < 0. 05 | *P* < 0. 001 | *P* < 0. 001 | |

# represent comparison with before irradiation, $P < 0.05$; * represent $P < 0.001$

**Table 4** The number and proportion of subclinical cardiac dysfunction in each period of the irradiation group

| | 1 week before irradiation (*n* = 18) | 3 month after irradiation (*n* = 18) | 6 month after irradiation (*n* = 12) | 12 month after irradiation (*n* = 6) |
|---|---|---|---|---|
| Relative decrease in GLS of > 15% | | | | |
| Irradiation group | - | 0 | 4 | 6 |
| Proportion | - | 0 | 33.3% | 100% |

(ICC) was 0. 84, 0. 87, and 0. 82 for GLS, LVEDV and LVESV (Table 6).

## Discussion

Radiotherapy remains a cornerstone in managing thoracic malignancies, including breast cancer, lung carcinoma, esophageal neoplasms, mediastinal lymphoma, and thymoma. However, contemporary RT modalities –even with technological advancements such as intensity-modulated radiotherapy and image-guided radiotherapy– cannot fully eliminate cardiac radiation exposure, as non-negligible cardiac radiation doses persist in most thoracic RT recipients.

Current understanding of RIHD primarily derives from observational clinical studies inherently confounded by heterogeneity in radiation fields, dosimetric parameters, treatment volume, and pre-existing cardiovascular comorbidities [1, 27, 28]. To establish causal relationships independent of these variables, controlled animal models become imperative. Canine models bridge a critical translational gap between rodent physiology and human cardiac pathophysiology, providing anatomically relevant platforms for longitudinal therapeutic investigations [29]. Our experimental approach employed single-fraction irradiation (20 Gy) to the left ventricle anterior wall in Beagle dogs– a species selected for their anatomically

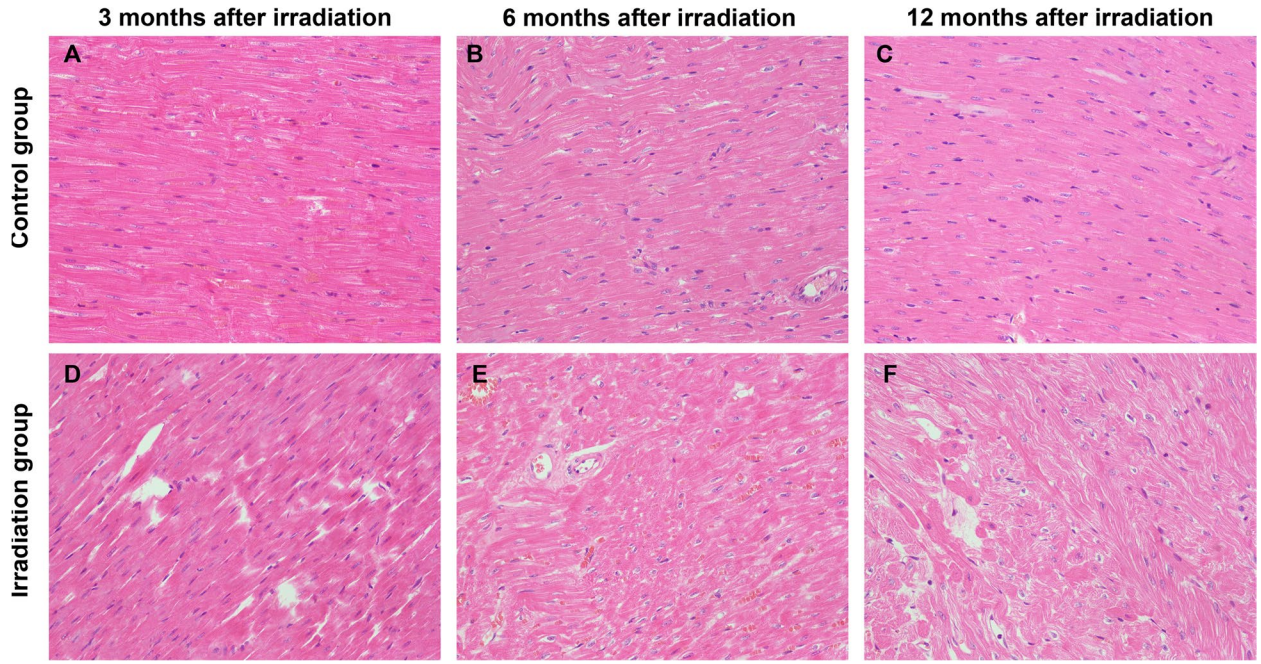


**Fig. 4** Hematoxylin–eosin staining of myocardium at 3 (**A**), 6 (**B**), and 12 month (**C**) after sham irradiation in the control group and at 3 (**D**), 6 (**E**), and 12 month (**F**) after irradiation in the irradiation group (magnification, ×400)

**Table 5** Comparison of histologic parameters between the control and irradiation groups

| Time | 3 month after irradiation | | | | | 6 month after irradiation | | | | | 12 month after irradiation | | | | |
|---|---|---|---|---|---|---|---|---|---|---|---|---|---|---|---|
| Grade | 0 | 1 | 2 | 3 | P | 0 | 1 | 2 | 3 | P | 0 | 1 | 2 | 3 | P |
| Myocardial degeneration | | | | | < 0. 001 | | | | | < 0. 001 | | | | | < 0. 001 |
| Control group | 28 | 2 | 0 | 0 | | 26 | 3 | 1 | 0 | | 24 | 4 | 2 | 0 | |
| Irradiation group | 4 | 24 | 2 | 0 | | 0 | 12 | 13 | 5 | | 0 | 2 | 7 | 21 | |
| Myocardial vascular injury | | | | | < 0. 001 | | | | | < 0. 001 | | | | | < 0. 001 |
| Control group | 26 | 3 | 1 | 0 | | 23 | 6 | 0 | 1 | | 20 | 7 | 2 | 1 | |
| Irradiation group | 9 | 17 | 2 | 2 | | 1 | 9 | 14 | 6 | | 0 | 4 | 14 | 12 | |

analogous cardiac geometry and adequate cardiac mass for 1) precise radiation targeting, 2) serial echocardiographic monitoring, and 3) STE analysis [30–34]. While fractionated low-dose regimens better approximate clinical radiotherapy protocols, the technical challenges of ensuring precise positional reproducibility across fractions led us to adopt a radiobiologically equivalent single high-dose paradigm, as validated by prior studies demonstrating comparable cardiac toxicity profiles between fractionated and hypofractionated regimens [35–38]. Histopathological validation confirmed successful RIHD modeling: Postmortem examination revealed radiation-dependent pathological progression characterized by 1) cardiomyocyte vacuolar degeneration, 2) diffuse interstitial fibrosis, and 3) concentric arteriolar wall thickening within irradiated myocardial segments. These findings not only corroborate the functional strain alterations detected by speckle tracking echocardiography but also establish histomorphological endpoints consistent with human RIHD manifestations.

The 2016 ESC position paper [14] recommends echocardiography as the first-line imaging modality for evaluating left ventricular systolic function in cancer patients undergoing cardiotoxic therapies. However, conventional echocardiography parameters lack the sensitivity to detect early-stage RIHD [39]. In contrast, STE – a novel echocardiographic technique developed over the past decade – enables quantitative assessment of myocardial deformation, thereby identifying subclinical alterations in left ventricular mechanics [11, 40–44]. Despite

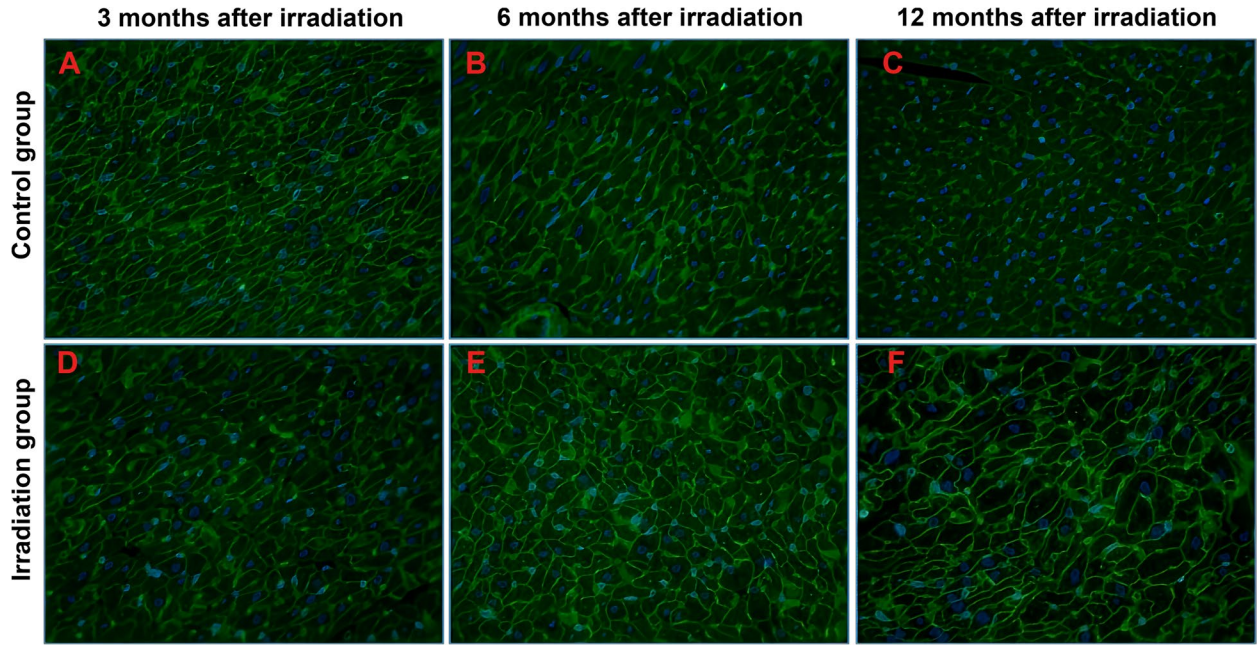


**Fig. 5** WGA staining of myocardium at 3 (**A**), 6 (**B**), and 12 month (**C**) after sham irradiation in the control group and at 3 (**D**), 6 (**E**), and 12 month (**F**) after irradiation in the irradiation group (magnification, ×400). Compared with the control group, the irradiated area showed various degrees of myocardial degeneration

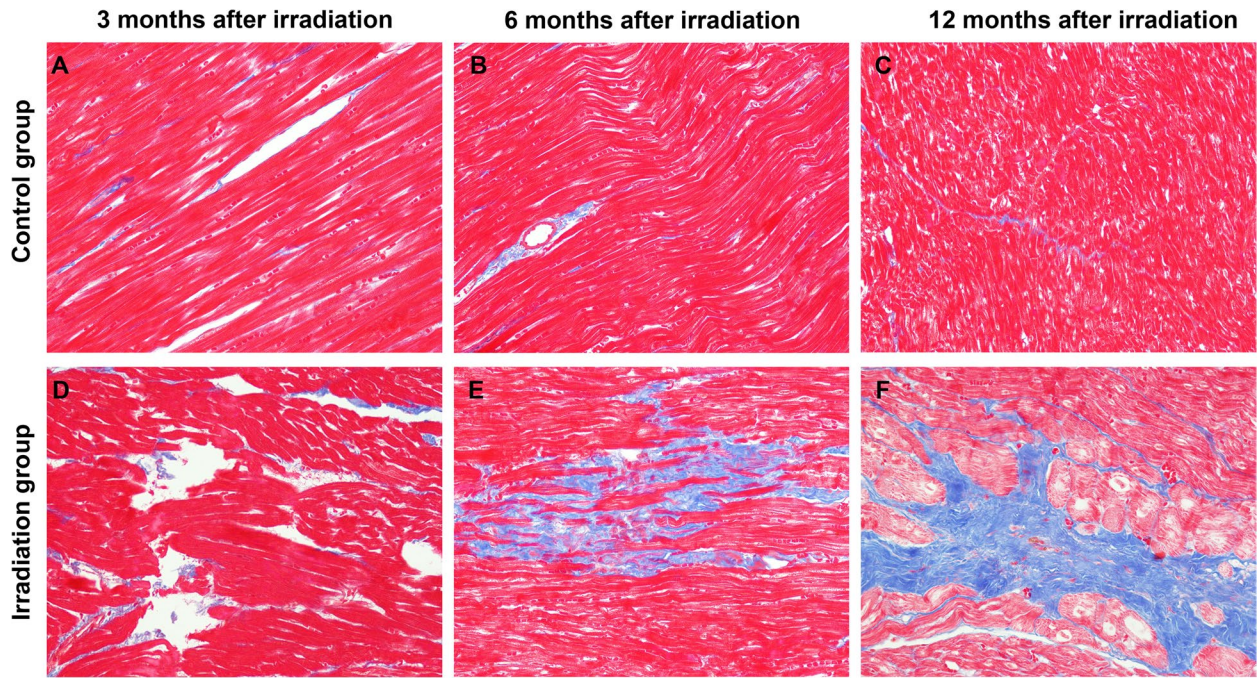


**Fig. 6** Masson staining of myocardium at 3 (**A**), 6 (**B**), and 12 month (**C**) after sham irradiation in the control group and at 3 (**D**), 6 (**E**), and 12 month (**F**) after irradiation in the irradiation group (magnification, ×400). Compared with the control group, myocardial interstitial fibrosis was aggravated progressively after irradiation in the irradiated area. The blue stained tissue was collagen fiber

**Table 6** Inter-observer and Intra-observer variability of GLS, LVEDV and LVESV

| | Inter-observer | | | Intra-observer | | |
|---|---|---|---|---|---|---|
| | Observer 1 | Observer 2 | ICC | Observer 1 | Observer 2 | ICC |
| GLS (%) | 19. 87 ± 0. 66 | 19. 92 ± 0. 63 | 0. 82 | 19. 87 ± 0. 66 | 19. 92 ± 0. 63 | 0. 84 |
| LVEDV (mm) | 30. 45 ± 3. 79 | 30. 4 ± 3. 21 | 0. 91 | 30. 45 ± 3. 79 | 30. 4 ± 3. 21 | 0. 87 |
| LVESV (mm) | 10. 4 ± 1. 18 | 10. 455 ± 1. 067 | 0. 85 | 10. 4 ± 1. 18 | 10. 455 ± 1. 067 | 0. 82 |

*ICC* intraclass correlation coefficient

its growing clinical adoption, few studies have systematically correlated STE-derived strain parameters with histopathological findings in the context of RIHD. To address this knowledge gap, our study employed a multimodal approach integrating 2D-STE, conventional echocardiography, and histopathological analysis in a Beagle dog model of RIHD. This experimental design allowed us to 1) characterize the temporal progression of radiation-induced cardiac dysfunction and 2) evaluate the diagnostic utility of STE in detecting early myocardial injury prior to overt functional decline.

At 3 months post-irradiation, subtle histopathological alterations were observed in the irradiated myocardium, including mild cardiomyocyte vacuolization, early-stage interstitial fibrosis, and reduced microvascular density. Concurrently, STE revealed significantly reduced GLS in irradiated segments, indicating subclinical myocardial dysfunction preceding conventional echocardiographic abnormalities. While diastolic dysfunction represents an early marker of cardiac injury, its non-regional specificity limits precise localization of radiation-induced damage. In contrast, segmental strain analysis (17-segment model) demonstrated spatially resolved mechanical impairment, with the most pronounced strain reduction correlating topographically with histopathological injury severity. In the irradiation group, the GLS and LS in the affected area continued to decline even after 6 and 12 months postradiation. At 12 months after irradiation, local cell wall motion abnormalities occurred in the irradiated area, and the segments with abnormal motion were consistent with the segments with the most severe strain reduction.

Radiation-induced posterior wall pathology manifested at 6- and 12-month follow-ups, accompanied by histopathological abnormalities in the posterior myocardium. This spatiotemporal progression indicates deteriorating myocardial dysfunction and reveals a spatially correlated relationship between echocardiographic strain reduction and histologic injury severity. Notably, subclinical cardiac dysfunction emerged in a subset of irradiated Beagles by 6 months, demonstrating radiation therapy's early cardiotoxic effects. These findings collectively demonstrate that 2D-STE achieves dual diagnostic capabilities: 1) detecting left ventricular functional alterations with precise spatial correspondence to pathological changes, and 2) enabling segmental quantification of myocardial injury extent while identifying subclinical dysfunction prior to conventional echocardiographic detection. This technical advantage enhances the accuracy of clinical surveillance and therapeutic decision-making for radiation-associated cardiotoxicity.

RIHD exhibits multi-compartment cardiac involvement, with delayed clinical manifestations including pericarditis, myocardial fibrosis, valvular lesions, coronary atherosclerosis, and conduction system abnormalities [45–47]. Myocardial fibrosis represents the terminal pathological endpoint in radiation cardiotoxicity, arising from progressive microvascular endothelial damage [48, 49]. Radiation-triggered endothelial injury initiates cytokine damage the microvasculature endothelium and increase the activation and reactive oxygen species overproduction, driving microvascular wall thickening, luminal stenosis, and perfusion impairment. This cascade culminates in chronic myocardial ischemia and subsequent fibrotic remodeling [1, 13, 50]. Our investigation systematically tracked radiation-induced myocardial pathology in Beagle dogs, demonstrating temporally progressive deterioration of cardiomyocyte integrity, interstitial fibrosis, and microvascular architecture..

Given the irreversible nature of established myocardial fibrosis, early RIHD detection prior to fibrotic transformation becomes clinically imperative. This study established that 2D-STE-derived GLS and LS reductions paralleled histopathological progression, enabling identification of preclinical myocardial injury before irreversible fibrotic deposition. While these findings position 2D-STE as a promising surveillance tool, future investigations must establish validated strain thresholds to guide targeted therapeutic interventions.

This studyemployed localized irradiation targeting the left ventricle anterior wall in Beagle dogs to establish a radiation cardiotoxicity model. However, 2D-STE analysis revealed LS reduction extending beyond the irradiated field into adjacent myocardial segments. This discrepancy may originate from inherent limitations in target delineation methodology: while based on the

standardized 17-segment left ventricular division for CT-guided planning, subjective interpretation during segmental border definition likely resulted in partial inclusion of lateral wall and anterior septal regions within the irradiated zone.

Existing evidence from clinical and preclinical studies [51–55] identifies serum cTnI elevation as an early biomarker of RIHD, typically normalizing months post-irradiation. Contrary to these reports, our serial cTnI measurements (3/6/12 months post-irradiation) showed no significant intergroup differences. This divergence likely reflects the temporal dynamics of biomarker sampling in our protocol, which may have captured the post-acute phase when cTnI levels had already returned to baseline. These observations highlight two critical limitations of cTnI monitoring: 1) transient detection windows requiring precise temporal alignment with injury phases, and 2) susceptibility to confounding clinical variables. Consequently, cTnI demonstrates insufficient specificity for longitudinal RIHD surveillance compared to spatially resolved STE biomarkers.

While cardiac magnetic resonance imaging (CMRI) with late gadolinium enhancement remains the gold standard for myocardial fibrosis assessment, its clinical utility is constrained by cost barriers, contraindications (e.g., renal insufficiency), and procedural complexity. Umezawa et al. [56] demonstrated CMRI's capability to detect radiation-induced myocardial fibrosis in esophageal cancer survivors, yet these technical limitations restrict routine implementation. Alternative modalities like PET/CT (e.g., 18F-FDG metabolic imaging by Yan et al. [57] and 13N-NH3 perfusion studies by Jianbo et al. [58]) enable early detection of radiation-induced myocardial abnormalities in canine models. However, PET/CT 's reliance on ionizing radiation and radiopharmaceutical administration precludes its use for longitudinal RIHD screening. In contrast, this study establishes 2D-STE as a clinically viable alternative, demonstrating some key advantages.Firstly, 2D-STE achieves dual diagnostic advantages: early identification of radiation-induced cardiotoxicity concurrent with initial histopathological alterations, combined with spatially resolved correlation between strain abnormalities and regions of peak radiation dose deposition. Furthermore, this modality demonstrates practical superiority through its non-invasive nature, cost-effectiveness, and elimination of cumulative radiation exposure risks. These attributes position 2D-STE as both a sensitive surveillance tool and a potential guide for targeted therapeutic interventions in RIHD management.

### Limitations

This study has inherent methodological constraints. First, the limited cohort size increases susceptibility to Type II statistical errors, potentially obscuring subtle radiation-induced pathophysiological changes. Second, the single-fraction radiation protocol diverges from clinical fractionated radiotherapy regimens, necessitating validation through studies employing hypofractionated dose simulations. Translation of these findings to human RIHD management requires multicenter clinical trials to establish standardized STE reference thresholds and intervention criteria.

## Conclusion

Radiation cardiotoxicity progression in Beagle dogs exhibited distinct temporal patterns: histopathological evidence of myocardial remodeling emerged by 3 months post-irradiation, progressing to irreversible fibrotic transformation at 12 months. The subclinical systolic dysfunction found by 2D-STE was highly consistent with the pathological changes, and segmental strain abnormalities first appeared in the area with the greatest degree of radiation involvement. These findings position 2D-STE as a non-invasive localization tool that 1) enables pre-fibrotic detection of radiation injury and 2) identifies myocardial regions receiving peak radiation dose deposition, thereby guiding time-sensitive therapeutic interventions before irreversible ventricular remodeling.

#### Abbreviations

| | |
|---|---|
| RIHD | Radiation-induced heart disease |
| GLS | Global longitudinal strain |
| LS | Longitudinal strain |
| 2D-STE | 2D speckle tracking echocardiography |
| LVEF | Left ventricular ejection fraction |
| IVSD | Interventricular septum end-diastolic dimension |
| LVPWD | Left ventricular posterior wall end-diastolic dimension |
| LVEDD | Left ventricular end-diastolic diameter |
| LVESD | Left ventricular end-systolic diameter |
| LVEDV | Left ventricular end-diastolic volume |
| LVESV | Left ventricular end-systolic volume |
| Peak E | Early diastolic peak velocity |
| Peak A | Late diastolic peak flow velocity |
| HE | Hematoxylin-eosin |
| WGA | Wheat germ agglutinin |
| ICC | Intra-class correlation coefficient |
| CMRI | Cardiac magnetic resonance imaging |

#### Acknowledgements

Not applicable.

#### Authors' contributions

All the authors read and approved the final manuscript. ZW, LL1 and LH designed the study. LH, ZW and LL2 collected the data. LL1, ZW, LH, CZ, LG and YL analyzed and discussed the data. LH and ZW performed the statistical analyses. ZW and LH drafted the manuscript and revised it according to the critical comments from CZ, YL, LG and LL1. LL1 corresponds to Ling-Min Liao. LL2 corresponds to Li-Qun Li. LL1 is the guarantor of this work and takes responsibility for the integrity of the data and the accuracy of the data analysis.

**Funding**
This work was supported by the National Natural Science Foundation of China [grant number 81960571] and Jiangxi Provincial Natural Science Foundation [grant number 20242BAB25550 and 20242BAB25518].

**Data availability**
All data generated or analysed during this study are included in this published article.

## Declarations

**Ethics approval and consent to participate**
Dedicated efforts were made to minimize animal suffering and the number of animals used is in accordance with the Guidelines for Animal Experiments of the Nanchang University, and which was approved by the Ethics Committee of Nanchang University, China, meanwhile the study was conducted and reported in accordance with the Animal Research: Reporting of In Vivo Experiments (ARRIVE) guidelines.

**Consent for publication**
Not applicable.

**Competing interests**
The authors declare no competing interests.

Received: 9 July 2024 Accepted: 6 March 2025
Published online: 20 March 2025

**References**

1. Mitchell JD, Cehic DA, Morgia M, Bergom C, Toohey J, Guerrero PA, et al. Cardiovascular manifestations from therapeutic radiation: a multidisciplinary expert consensus statement from the international cardio-oncology society. JACC CardioOncol. 2021;3(3):360–80. https://doi.org/10.1016/j.jaccao.2021.06.003.
2. Wang H, Wei J, Zheng Q, Meng L, Xin Y, Yin X, et al. Radiation-induced heart disease: a review of classification, mechanism and prevention. Int J Biol Sci. 2019;15(10):2128–38. https://doi.org/10.7150/ijbs.35460.
3. Sárközy M, Varga Z, Gáspár R, Szűcs G, Kovács MG, Kovács ZZA, et al. Pathomechanisms and therapeutic opportunities in radiation-induced heart disease: from bench to bedside. Clin Res Cardiol. 2021;110(4):507–31. https://doi.org/10.1007/s00392-021-01809-y.
4. Menezes KM, Wang H, Hada M, Saganti PB. Radiation matters of the heart: a mini review. Front Cardiovasc Med. 2018;5:83. https://doi.org/10.3389/fcvm.2018.00083.
5. Trivedi SJ, Tang S, Byth K, Stefani L, Lo Q, Otton J, et al. segmental cardiac radiation dose determines magnitude of regional cardiac dysfunction. J Am Heart Assoc. 2021;10(7):e019476. https://doi.org/10.1161/JAHA.120.019476.
6. Davis KS. Intrathoracic change following X-ray treatment:a clinical and experimental study. Radiology. 1924;3(5):301–22. https://doi.org/10.1148/3.4.301.
7. Wang KX, Ye C, Yang X, Ma P, Yan C, Luo L. New insights into the understanding of mechanisms of radiation-induced heart disease. Curr Treat Options Oncol. 2023;24(1):12–29. https://doi.org/10.1007/s11864-022-01041-4.
8. Siegel RL, Miller KD, Wagle NS, Jemal A. Cancer statistics, 2023. CA Cancer J Clin. 2023;73(1):17–48. https://doi.org/10.3322/caac.21763.
9. Siegel RL, Miller KD, Fuchs HE, Jemal A. Cancer statistics, 2022. CA Cancer JClin. 2022;72(1):7–33. https://doi.org/10.3322/caac.21708.
10. Polomski ES, Antoni ML, Jukema JW, Kroep JR, Dibbets-Schneider P, Sattler MGA, et al. Nuclear medicine imaging methods of radiation-induced cardiotoxicity. Semin Nucl Med. 2022;52(5):597–610. https://doi.org/10.1053/j.semnuclmed.2022.02.001.
11. Li T, Zhuang H, Wang Y, Li J, Zhu D, Cui M. Two-dimensional speckle tracking echocardiography in evaluating radiation-induced heart damage. Asia Pac JOncol Nurs. 2021;9(2):119–24. https://doi.org/10.1016/j.apjon.2021.12.008.
12. Ping Z, Peng Y, Lang H, Xinyong C, Zhiyi Z, Xiaocheng W, et al. Oxidative stress in radiation-induced cardiotoxicity. Oxid Med Cell Longev. 2020;2020:3579143. https://doi.org/10.1155/2020/3579143.PMID:32190171;PMCID:PMC7071808.
13. Zhu D, Li T, Zhuang H, Cui M. Early detection of cardiac damage by two-dimensional speckle tracking echocardiography after thoracic radiation therapy: study protocol for a prospective cohort study. Front Cardiovasc Med. 2022;8:735265. https://doi.org/10.3389/fcvm.2021.735265.
14. Hoeller U, Borgmann K, Oertel M, Haverkamp U, Budach V, Eich HT. Late sequelae of radiotherapy—The effect of technical and conceptual innovations in radiation oncology. Dtsch Arztebl Int. 2021;118(12):205–11. https://doi.org/10.3238/arztebl.m2021.0024.1.
15. Belzile-Dugas E, Eisenberg MJ. Radiation-induced cardiovascular disease: review of an underrecognized pathology. J Am Heart Assoc. 2021;10(18):e021686. https://doi.org/10.1161/JAHA.121.021686.
16. Wang X, Palaskas NL, Yusuf SW, Abe JI, Lopez-Mattei J, Banchs J, et al. Incidence and onset of severe cardi ac events after radiotherapy for esophageal cancer. J Thorac Oncol. 2020;15(10):1682–90. https://doi.org/10.1016/j.jtho.2020.06.014.
17. Son C, Moey MYY, Walker PR, Naqash AR, Peach MS, Ju AW. Cardiac toxicity in patients with lung cancer receiving thoracic radiotherapy and immunotherapy. Front Oncol. 2023;12:1025455. https://doi.org/10.3389/fonc.2022.1025455.
18. Vallerio P, Maloberti A, Palazzini M, Occhi L, Peretti A, Nava S, et al. Thoracic radiotherapy as a risk factor for heart ischemia in subjects treated with chest irradiation and chemotherapy and without classic cardiovascular RISK factors. Radiother Oncol. 2020;152:146–50. https://doi.org/10.1016/j.radonc.2020.07.004.
19. Clasen SC, Shou H, Freedman G, Plastaras JP, Taunk NK, Kevin Teo BK, et al. Early cardiac effects of contemporary radiation therapy in patients with breast cancer. Int J Radiat Oncol Biol Phys. 2021;109(5):1301–10. https://doi.org/10.1016/j.ijrobp.2020.12.008.
20. Lancellotti P, Nkomo VT, Badano LP, Bergler-Klein J, Bogaert J, Davin L, et al. Expert consensus for multi-modality imaging evaluation of cardiovascular complications of radiotherapy in adults:a report from the European Association of Cardiovascular Imaging and theAmerican Society of Echocardiography. J Am Soc Echocardiogr. 2013;26(9):1013–32. https://doi.org/10.1016/j.echo.2013.07.005.
21. Zamorano JL, Lancellotti P, Rodriguez Muñoz D, Aboyans V, Asteggiano R, Galderisi M, et al. 2016 ESC Position Paper on cancer treatments and cardiovascular toxicity developed under the auspices of the ESC Committee for Practice Guidelines: The Task Force for cancer treatments and cardiovascular toxicity of the European Society of Cardiology (ESC). Eur Heart J. 2016;37(36):2768–801. https://doi.org/10.1093/eurheartj/ehw211.
22. Tanaka S, Shibuya H, Suzuki S, Kanno N, Harada Y, Sato A, et al. Long-term administration of prednisolone: effects on the myocardial tissue of healthy beagle dogs. J Vet Med Sci. 2021;83(1):84–93. https://doi.org/10.1292/jvms.20-0401.
23. Tokatli F, Uzal C, Doganay L, Kocak Z, Kaya M, Ture M, et al. The potential cardioprotective effects of amifostine in irradiated rats. Int J Radiat Oncol Biol Phys. 2004;58(4):1228–34. https://doi.org/10.1016/j.ijrobp.2003.09.071.
24. Dogan I, Sezen O, Sonmez B, Zengin AY, Yenilmez E, Yulug E, et al. Myocardial perfusion alterations observed months after radiotherapy are related to the cellular damage. Nuklearmedizin. 2010;49(6):209–15. https://doi.org/10.3413/nukmed-0315-10-05.
25. Chen D, Yu W, Zhong C, Hong Q, Huang G, Que D, et al. Elabela ameliorates doxorubicin-induced cardiotoxicity by promoting autophagic flux through TFEB pathway. Pharmacol Res. 2022;178:106186. https://doi.org/10.1016/j.phrs.2022.106186.
26. Singh VP, Le B, Khode R, Baker KM, Kumar R. Intracellular angiotensin II production in diabetic rats is correlated with cardiomyocyte apoptosis, oxidative stress, and cardiacfibrosis. Diabetes. 2008;57(12):3297–306. https://doi.org/10.2337/db08-0805.
27. Schlaak RA, SenthilKumar G, Boerma M, Bergom C. Advances in preclinical research models of radiation-induced cardiac toxicity. Cancers (Basel). 2020;12(2):415. https://doi.org/10.3390/cancers12020415.
28. Xu X, Wang D, Yin Y, Wang Q, Dai H, Chen L, et al. Role of global longitudinal strain in evaluating radiotherapy–induced early cardiotoxicity in breast cancer: a meta-analysis. Kardiol Pol. 2023;81(1):58–60. https://doi.org/10.33963/KP.a2022.0274.

29. Boss MK. Canine comparative oncology for translational radiation research. Int J Radiat Biol. 2022;98(3):496–505. https://doi.org/10.1080/09553002.2021.1987572.
30. Sharma S, Moros EG, Boerma M, Sridharan V, Han EY, Clarkson R, et al. A novel technique for image-guided local heart irradiation in the rat. Technol Cancer Res Treat. 2014;13(6):593–603. https://doi.org/10.7785/tcrtexpress.2013.600256.
31. Dreyfuss AD, Velalopoulou A, Avgousti H, Bell BI, Verginadis II. Preclinical models of radiation-induced cardiac toxicity: potential mechanisms and biomarkers. Front Oncol. 2022;12:920867. https://doi.org/10.3389/fonc.2022.920867.
32. de Almeida MC, Macías Y, Tretter JT, Sánchez-Quintana D, Cabrera JA, Spicer DE, et al. Similarities and differences in thearrangement of the atrioventricular conduction axis in the canine compared to the human heart. Heart Rhythm. 2021;18(11):1990–8. https://doi.org/10.1016/j.hrthm.2021.07.065.
33. Sayseng V, Ober RA, Grubb CS, Weber RA, Konofagou E. Monitoring canine myocardial infarction formation and recovery via transthoracic cardiac strain imaging. Ultrasound Med Biol. 2020;46(10):2785–800. https://doi.org/10.1016/j.ultrasmedbio.2020.06.010.
34. Kruckman-Gatesy CR, Ames MK, Griffin LR, Boss MK, Rao S, Leary D, et al. A retrospective analysisof stereotactic body radiation therapy for canine heart base tumors: 26 cases. JVetCardiol. 2020;27:62–77. https://doi.org/10.1016/j.jvc.2020.01.002.
35. DeBo RJ, Lees CJ, Dugan GO, Caudell DL, Michalson KT, Hanbury DB, et al. Late effects of total-body gamma irradiation on cardiac structure and function in male rhesus macaques. Radiat Res. 2016;186(1):55–64. https://doi.org/10.1667/RR14357.1.
36. Tewart JR, Fujardo LF, Cohn KE, Page V. Experimental radiation-induced heart disease in rabbits. Radiology. 1968;91(4):814–7. https://doi.org/10.1148/91.4.814.
37. Boerma M, Sridharan V, Krager KJ, Pawar SA. Small animal models of localized heart irradiation. Methods Cell Biol. 2022;168:221–34. https://doi.org/10.1016/bs.mcb.2021.12.016.
38. Li P, Chen F, Sun XY, Wang B, Yang M. Advances in experimental research on radiation-induced heart injury in animal models. Chin J Radiol Health. 2020;29(01):93–7. https://doi.org/10.13491/j.issn.1004-714X.2020.01.022.
39. Cobarro Gálvez L, Arbas Redondo E, Contreras Lorenzo C, López FT. Advanced echocardiographic techniques in cardio-oncology: the role for early detection of cardiotoxicity. Curr Cardiol Rep. 2022;24(9):1109–16. https://doi.org/10.1007/s11886-022-01728-y.
40. Trivedi SJ, Choudhary P, Lo Q, Sritharan HP, Iyer A, Batumalai V, et al. Persistent reduction in global longitudinal strain in the longer term after radiation therapy in patients with breast cancer. Radiother Oncol. 2019;132:148–54. https://doi.org/10.1016/j.radonc.2018.10.023.
41. Quintana RA, Bui LP, Moudgil R, Palaskas N, Hassan S, Abe JI, et al. Speckle-tracking echocardiographyin cardio-oncology and beyond. Tex Heart Inst J. 2020;47(2):96–107. https://doi.org/10.14503/THIJ-18-6736.
42. McGregor PC, Moura FA, Banchs J, Aragam JR. Role of myocardial strain imaging in surveillance and management of cancer therapeutics-related cardiac dysfunction: a systematic review. Echocardiography. 2021;38(2):314–28. https://doi.org/10.1111/echo.14944.
43. Quinaglia T, Gongora C, Awadalla M, Hassan MZO, Zafar A, Drobni ZD, et al. Global circumferential and radial strain among patients with immune checkpoint inhibitor myocarditis. JACC Cardiovasc Imaging. 2022;15(11):1883–96. https://doi.org/10.1016/j.jcmg.2022.06.014.
44. Araujo-Gutierrez R, Chitturi KR, Xu J, Wang Y, Kinder E, Senapati A, et al. Baseline global longitudinal strain predictive of anthracycline-induced cardiotoxicity. Cardiooncology. 2021;7(1):4. https://doi.org/10.1186/s40959-021-00090-2.
45. Venneri L, Zoppellaro G, Khattar RS. Cardio-oncology: the role of advanced echocardiography in cancer patients. Expert Rev Cardiovasc Ther. 2018;16(4):249–58. https://doi.org/10.1080/14779072.2018.1443394.
46. Šteiner I. Pathology of radiation induced heart disease. Rep Pract Oncol Radiother. 2020;25(2):178–81. https://doi.org/10.1016/j.rpor.2019.12.015.
47. Quintero-Martinez JA, Cordova-Madera SN, Villarraga HR. Radiation-Induced Heart Disease. J. Clin Med. 2021;11(1):146. https://doi.org/10.3390/jcm11010146.
48. Hendry JH, Akahoshi M, Wang LS, Lipshultz SE, Stewart FA, Trott KR. Radiation-induced cardiovascular injury. Radiat Environ Biophys. 2008;47(2):189–93. https://doi.org/10.1007/s00411-007-0155-7.
49. Tapio S. Pathology and biology of radiation-induced cardiac disease. J Radiat Res. 2016;57(5):439–48. https://doi.org/10.1093/jrr/rrw064.
50. Kirova Y, Tallet A, Aznar MC, Loap P, Bouali A, Bourgier C. Radio-induced cardiotoxicity: from physiopathology and risk factors to adaptation of radiotherapy treatment planningandrecommended cardiac follow-up. Cancer Radiother. 2020;24(6–7):576–85. https://doi.org/10.1016/j.canrad.2020.07.001.
51. Cardinale D, Sandri MT, Colombo A, Colombo N, Boeri M, Lamantia G, et al. Prognostic value of troponin I in cardiac risk stratification of cancer patients undergoing high-dose chemotherapy. Circulation. 2004;109(22):2749–54. https://doi.org/10.1161/01.CIR.0000130926.51766.CC.
52. Xu T, Meng QH, Gilchrist SC, Lin SH, Lin R, Xu T, et al. Assessment of prognostic value of high-sensitivity cardiac troponin t for early prediction of chemoradiation therapy-induced cardiotoxicity in patients with non-small cell lung cancer: a secondary analysis of a prospective randomized trial. Int J Radiat Oncol Biol Phys. 2021;111(4):907–16. https://doi.org/10.1016/j.ijrobp.2021.07.035.
53. Tzolos E, Adamson PD, Hall PS, Macpherson IR, Oikonomidou O, MacLean M, et al. Dynamic changes in high-sensitivitycardiac troponin i in response to anthracycline-based chemotherapy. Clin Oncol (R Coll Radiol). 2020;32(5):292–7. https://doi.org/10.1016/j.clon.2019.11.008.
54. Gkantaifi A, Papadopoulos C, Spyropoulou D, Toumpourleka M, Iliadis G, Kardamakis D, et al. Breast Radiotherapy and early adverse cardiac effects. The role of serum biomarkers and strain echocardiography. Anticancer Res. 2019;39(4):1667–73. https://doi.org/10.21873/anticanres.13272.
55. Skyttä T, Tuohinen S, Boman E, Virtanen V, Raatikainen P, Kellokumpu-Lehtinen PL. Troponin T-release associates with cardiac radiation doses during adjuvant left-sided breast cancer radiotherapy. RadiatOncol. 2015;10:141. https://doi.org/10.1186/s13014-015-0436-2.
56. Umezawa R, Ota H, Takanami K, Ichinose A, Matsushita H, Saito H, et al. MRI findings of radiation-induced myocardial damage in patients with oesophageal cancer. Clin Radiol. 2014;69(12):1273–9. https://doi.org/10.1016/j.crad.2014.08.010.
57. Yan R, Song J, Wu Z, Guo M, Liu J, Li J, et al. Detection of myocardial metabolic abnormalitiesby 18F-FDG PET/CT and corresponding pathological changes in beagles withlocal heart irradiation. Korean J Radiol. 2015;16(4):919–28. https://doi.org/10.3348/kjr.2015.16.4.919.
58. Song J, Yan R, Wu Z, Li J, Yan M, Hao X, et al. 13N-Ammonia PET/CT detection of myocardial perfusion abnormalities in beagle dogs after local heart irradiation. J Nucl Med. 2017;58(4):605–10. https://doi.org/10.2967/jnumed.116.179697.


## Publisher's Note